PHYS 4909 Final Report

A Numerical Exploration of Two Neutrino Mass Generation Models

Aya Tessier

Date Submitted: April 25, 2025 Supervisor: Dr. Seyda Ipek

Abstract

Neutrinos are extremely light particles that undergo flavor oscillations due to their masses, masses which are unexplained by the Standard Model (SM). This analysis sought numerical solutions for two previously existing neutrino mass generation models that blend supersymmetry and the Inverse Seesaw mechanism. The first model is analytically solvable but requires one massless SM neutrino. The second model allows all three SM neutrinos to be massive but is underconstrained and requires a major simplication to solve analytically. Using MATLAB, previous analytical solutions for each model were found numerically and a method for obtaining solutions without major simplifications was developed for the second model. The results found predict decay signatures that may be investigated in future collider experiments, and target regions of interest in the underconstrained parameter space. These solutions fit known neutrino oscillation and cosmological constraints.

1 Theory

1.1 Neutrino Oscillations

Neutrinos are by far the lightest of the massive particles found in the Standard Model of particle physics. They come in the three leptonic flavors (electron, muon and tau) and rarely interact: of the billions passing through every square centimeter of stuff on Earth per second, only a small handful will react with other matter. Most neutrinos that are observed on Earth are produced from the fusion process in the interior of the Sun or high-energy cosmic rays producing particle showers when they interact with the atmosphere. Neutrinos can also be generated in abundance from nuclear reactors and experiments.

Curiously, according to the Standard Model, all neutrinos should be massless. The first experiment to contradict this theory was preformed in 1968 by Ray Davis[1]. This experiment measured electron neutrinos produced by the Sun over a period of months by flushing about 30 argon atoms out of 615 metric ton tank of chlorine. This was only a third of the predicted yield. With such small numbers the scientific community was skeptical until other experiments started to independently confirm these results, verifying what came to be known as *The Solar Neutrino Problem*[2].

The mechanism explaining the "missing" neutrinos was proposed that same year by Pontecorvo and Gribov, [3]. If the three neutrino flavour states were not eigenstates of the Hamiltonian, they would evolve over time. If this was the case, electron neutrinos would oscillate to another state during the flight to Earth, and explain why fewer signals were seen by electron-neutrino-sensitive experiments.

The flavour oscillations of the Solar Neutrino Problem can be well approximated as mixing between two flavour states: ν_e and a linear combination state of ν_μ and ν_τ (denoted by ν_μ in the subsequent example) [4]. The basis of the two flavour states $\{|\nu_e\rangle, |\nu_\mu\rangle\}$ and two mass states $\{|\nu_1\rangle, |\nu_2\rangle\}$, which are the eigenstates of the Hamiltonian, are related by a unitary rotation matrix, U, which depends on the mixing angle θ between the flavour eigenstates.

$$U_{\alpha i} = \begin{pmatrix} U_{e1} & U_{e2} \\ U_{\mu 1} & U_{\mu 2} \end{pmatrix} = \begin{pmatrix} \cos \theta & \sin \theta \\ -\sin \theta & \cos \theta \end{pmatrix}, \ |\nu_{\alpha}\rangle = \sum_{i=1,2} U_{\alpha i} |\nu_{i}\rangle \tag{1}$$

Starting with the initial electron neutrino produced in the Sun, the state evolves in time as

$$|\psi(t)\rangle = \hat{T}(t)|\psi(0)\rangle = \exp\left(\frac{-i\hat{H}t}{\hbar}\right)|\nu_e\rangle = \exp\left(\frac{-iE_1t}{\hbar}\right)\cos\theta|\nu_1\rangle + \exp\left(\frac{-iE_2t}{\hbar}\right)\sin\theta|\nu_2\rangle$$
 (2)

where E_i are eigenvalues of the Hamiltonian for the two mass eigenstates. For most practical applications it is best to reformulate this state in terms of the distance L that the neutrino travels. Assuming that the electron neutrino is ultra-relativistic $\left(E = \sqrt{|\mathbf{p}|^2 c^2 + m_i^2 c^4} \approx |\mathbf{p}|c\right)$ and it has a constant energy E

$$E_{i}^{2} = |\mathbf{p}|^{2}c^{2} + m_{i}^{2}c^{4} = |\mathbf{p}|^{2}c^{2}\left(1 + \frac{m_{i}^{2}c^{2}}{|\mathbf{p}|^{2}}\right)$$

$$E_{i} \approx |\mathbf{p}|c\left(1 + \frac{m_{i}^{2}c^{2}}{2|\mathbf{p}|^{2}}\right) \approx E + \frac{m_{i}^{2}c^{4}}{2E}$$
(3)

$$L \approx ct$$
 (4)

We can then calculate the probability that this neutrino is still in the electron flavour state upon measurement. Substituting for E_1 and E_2

$$\langle \nu_e | \psi(t) \rangle = \cos^2 \theta \, \exp \left(\frac{-iE_1 t}{\hbar} \right) + \sin^2 \theta \, \exp \left(\frac{-iE_2 t}{\hbar} \right)$$

$$P_{e \to e} = |\langle \nu_e | \psi(0) \rangle|^2$$

$$= \left| \cos^2 \theta \exp\left(\frac{-iE_1 t}{\hbar}\right) + \sin^2 \theta \exp\left(\frac{-iE_2 t}{\hbar}\right) \right|^2$$

$$= 1 - \sin^2(2\theta) \sin^2\left(\frac{E_2 - E_1}{2\hbar}t\right)$$

$$P_{e \to e} = 1 - \sin^2(2\theta) \sin^2\left(\frac{m_2^2 - m_1^2}{4\hbar E}c^3L\right)$$
(5)

and

$$P_{e \to \mu} = 1 - P_{e \to e} = \sin^2(2\theta) \sin^2\left(\frac{m_2^2 - m_1^2}{4\hbar E}c^3L\right). \tag{6}$$

By collecting data for various distances and neutrino energies, it is possible to solve for the mixing angle and mass squared difference $m_i^2 - m_j^2 = \Delta m_{ij}^2$.

Most early neutrino detectors were focused on solving the solar neutrino problem. The Kamiokande and Super Kamiokande experiments in Japan studied solar neutrinos with energies > 5.0 - 7.5 MeV by looking for the Cherenkov radiation in water that was produced when neutrinos underwent an elastic scattering reaction [5]

$$\nu + e^- \to \nu + e^-. \tag{7}$$

In these experiments, all neutrinos can scatter by exchange of a Z-boson but only electron neutrinos can scatter with a W-boson, a reaction with a larger cross-section. This leads to an elastic scattering flux with an 85% lesser contribution from muon and tau neutrinos.

$$\Phi_{\text{elastic}} \propto \Phi_{\nu_e} + 0.15 \left(\Phi_{\nu_\mu} + \Phi_{\nu_\tau} \right) \tag{8}$$

Super-K only measured 45% of the neutrino flux predicted by the best models of solar fusion [5]. If correct, it meant that 65% of the original electron neutrinos had changed flavours before being detected on Earth. The final piece of evidence confirming neutrino oscillations came in 2002 when the Sudbury Neutrino Observatory (SNO) in Sudbury, Canada confirmed the hypothesis by measuring the flux of electron neutrinos in conjunction with the elastic scattering flux [6]. Unlike the Kamiokande experiments, SNO used heavy water permitting two additional reactions: charged current, exclusive to only electron neutrinos

$$\nu_e + {}^2\mathrm{H} \to p + p + e^- \tag{9}$$

and neutral current, for all neutrinos

$$\nu + {}^{2}\mathrm{H} \to p + n + \nu \tag{10}$$

Using the elastic, charged current, and neutral current reactions, SNO was able to confirm that 2/3 of the electrons neutrinos in the Sun had undergone a flavour oscillation (figure 1). The KamLAND experiment in Japan independently confirmed electron neutrino oscillations by measuring antineutrinos produced in nuclear reactors [7]. The mass squared difference and mixing angle found were $\theta_{\rm sol} \approx 35^{\circ}$ and $\Delta m_{\rm sol}^2 \simeq 8 \times 10^{-5} \, {\rm eV}^2$ [2].

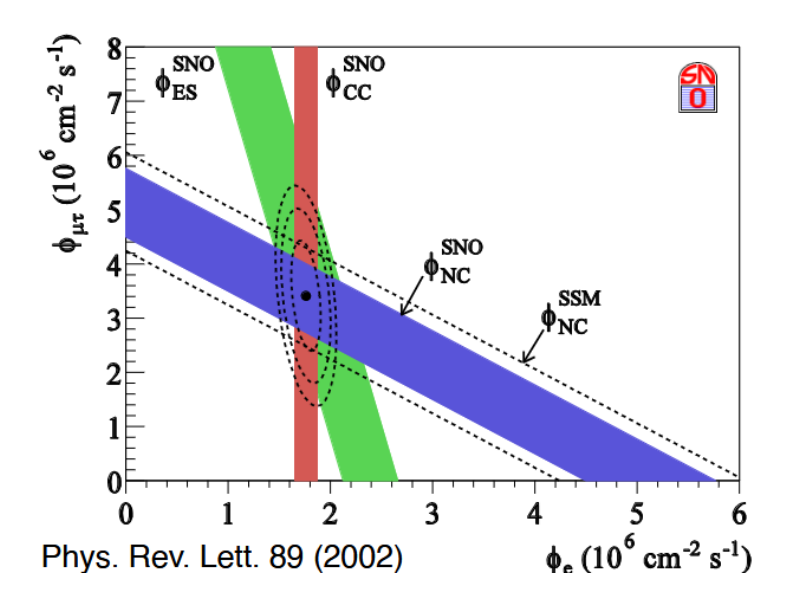


Figure 1: Comparison of neutrino fluxes from the three different reactions observed at SNO (width = $\pm 1\sigma$) [6]. The diagonal dashed lines indicate the Solar Standard Model (SSM) theoretical prediction of neutrino production. Their intersection matches the fit values consistent with oscillations occurring.

The Kamiokande experiments were also searching for muon neutrino oscillations from cosmic ray collisions in the upper atmosphere. Pions formed in these collisions will create muons and muon neutrinos with energies between $10^8 - 10^{10} \text{eV}$

$$\pi^+ \to \mu^+ + \nu_\mu, \ \pi^- \to \mu^- + \bar{\nu}_\mu$$
 (11)

Muons at "lower" energies may also decay into electron and muon neutrinos.

$$\mu^+ \to e^+ + \nu_e + \bar{\nu}_{\mu}, \quad \mu^- \to e^- + \bar{\nu}_e + \nu_{\mu}$$
 (12)

The cosmic ray flux is mostly isotropic, meaning that an equal number of muon neutrinos should be coming in all directions after striking Earth's atmosphere. However, muon neutrinos produced above the detector quickly travel to the detector without time to oscillate, but those coming in the opposite direction must travel Earth's entire diameter. Able to measure the direction of the neutrinos, Kamiokande found roughly a 2:1 ratio of muon to electron neutrinos overhead, while a much lower ratio from the opposite direction. In this case, the muon neutrinos were oscillating into tau neutrinos as they passed through the Earth. This scenario can once again be modeled as a two-generation mixing as no additional electron neutrinos were produced.

$$\theta_{\rm atm} \approx 45^{\circ}$$
 (13)

$$\theta_{\rm atm} \approx 45^{\circ}$$
 (13)
 $\Delta m_{\rm atm}^2 \simeq 3 \times 10^{-3} \,\mathrm{eV}^2$

1.2Experimental Constraints

Multiple other experiments have leveraged different length and energy scales to probe neutrino oscillations. The case of three neutrinos can be described by three mixing angles θ_{12} , θ_{13} , θ_{23} and two mass squared differences Δm_{21}^2 , Δm_{3l}^2 (the third can be written in terms of the other differences). The 3l notation comes from inherent ambiguity in the mass hierarchy of the mass eigenstates. Since oscillation experiments only measure relative mass differences, ν_3 may be the heaviest or lightest eigenstate. This creates two possible scenarios: normal- and inverted-hierarchy (figure 2a). The measured differences are $\Delta m_{21}^2 \simeq \Delta m_{\rm sol}^2$ and $\Delta m_{3l}^2 \simeq \Delta m_{\rm atm}^2$.

The mixing matrix that describes the transformation between the three mass and flavour eigenstates is known as the Pontecorvo–Maki–Nakagawa–Sakata (PMNS) matrix and is parameterized by the three mixing angles (eqn. 15) [8]. For the purposes of this discussion the CP-violation phase $\delta = 0$. This matrix is analogous in function to the Cabibbo-Kobayashi-Maskawa matrix which describes quark mixing via the weak interaction.

$$U = \begin{pmatrix} c_{12} & s_{12}c_{13} & s_{13}e^{i\delta} \\ -s_{12}c_{23} - c_{12}s_{23}s_{13}e^{i\delta} & c_{12}c_{23} - s_{12}s_{23}s_{13}e^{i\delta} & s_{23}c_{13} \\ s_{12}s_{23} - c_{12}c_{13}s_{13}e^{i\delta} & -c_{12}s_{23} - s_{12}c_{23}s_{13}e^{i\delta} & c_{23}c_{13} \end{pmatrix}, c_{ij} \equiv \cos\theta_{ij}, s_{ij} \equiv \sin\theta_{ij}$$
 (15)

The terms $\theta_{12} \approx \theta_{sol}$, and $\theta_{23} \approx \theta_{atm}$ which are much greater in size than $\theta_{13} < 10^{\circ}$. The PMNS matrix also tells us the flavour composition of the mass eigenstates (figure 2b).

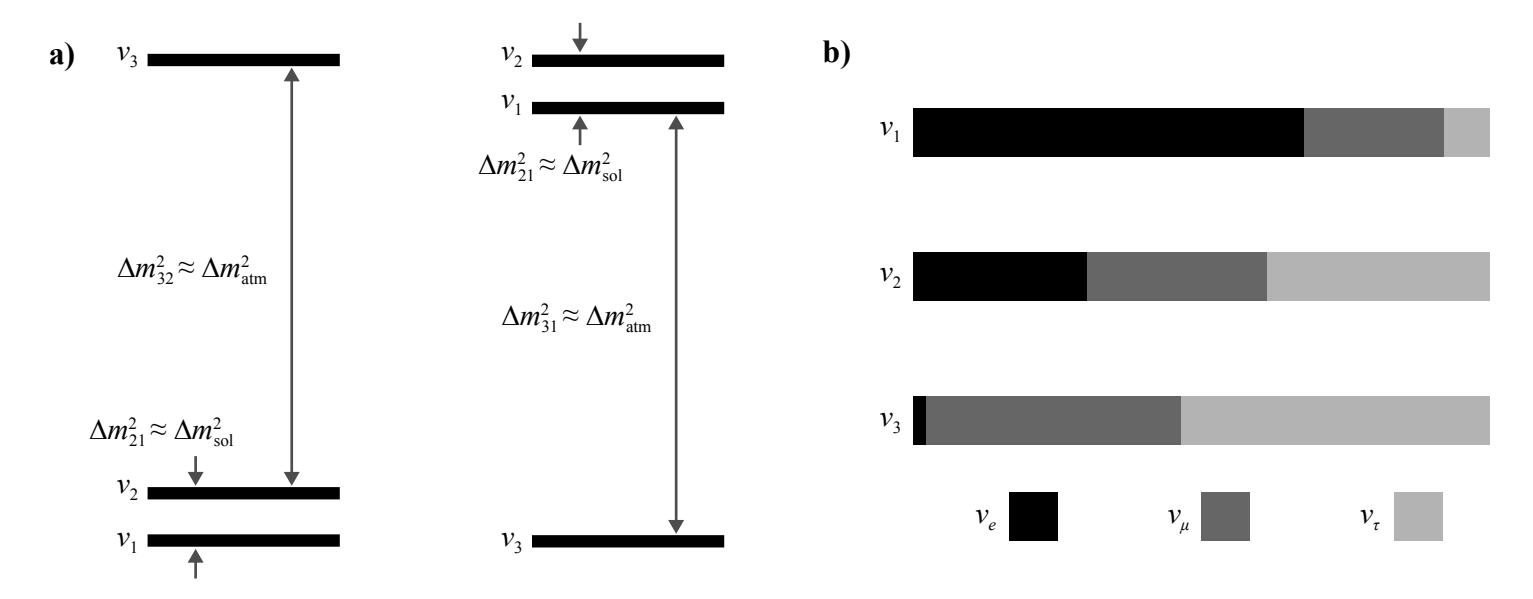


Figure 2: a) Normal (left) and inverted (right) hierarchies of the three neutrino mass eigenstates ν_1 , ν_2 , ν_3 (not to scale). b) Flavour composition of the three mass eigenstates found from the PMNS matrix elements (data from [9]).

The values of the mixing angles and mass squared differences used in this analysis are taken from publications from NuFIT, an organization that provides "[A]n updated global analysis of neutrino oscillation measurements". The specific values below are referenced from the NuFIT 5.3 release (including the Super Kamiokande atmospheric data) [9](www.nu-fit.org).

$$\theta_{12} = 33.67^{+0.73}_{-0.71} \,\text{deg}, \ \theta_{13} = 8.58^{+0.11}_{-0.11} \,\text{deg}, \ \theta_{23} = 42.3^{+0.1.1}_{-0.9} \,\text{deg}$$
 (16)

$$|\Delta m_{21}|^2 = (7.41^{+0.21}_{-0.20}) 10^{-5} \text{eV}^2, \ |\Delta m_{31}|^2 = (2.505^{+0.024}_{-0.026}) 10^{-3} \text{eV}^2$$
 (17)

To find the 1σ confidence intervals on the individual PMNS elements, a numerical scan was preformed by varying each mixing angle between its confidence bounds. For each element, the maximum and minimum value found in the scan gave the error bound ($\delta = 0$).

$$U_{\text{PMNS}} = \begin{pmatrix} 0.82_{-0.007}^{+0.007} & 0.55_{-0.011}^{+0.010} & 0.15_{-0.002}^{+0.002} \\ -0.49_{-0.012}^{+0.014} & 0.56_{-0.019}^{+0.017} & 0.67_{-0.012}^{+0.014} \\ 0.28_{-0.017}^{+0.018} & -0.62_{-0.015}^{+0.013} & 0.73_{-0.013}^{+0.011} \end{pmatrix}$$

$$(18)$$

Two other constraints can be placed on the neutrino mass. Using measurements of baryon acoustic oscillations, the DESI collaboration have put an upper limit on the sum of the neutrino masses at $\sum m_{\nu} < 0.064$ eV assuming the Λ CDM model of the universe [10]. Another experiment, KATRIN, is attempting to directly measure the scale of the SM neutrino masses and has recently put an upper bound on the heaviest neutrino mass at $m_3 < 0.5$ eV [11]. The DESI result is still much more constraining but KATRIN is expected to continue lowering the upper bound and possibly discover the actual value of the heaviest SM neutrino state.

1.3 New Physics

In the Standard Model all fermions such as electrons, quarks, etc., can be described as being left- or right-handed. These are known as Dirac fermions and can gain mass by the Higgs mechanism which switches their handedness. As the SM neutrinos are only left-handed (antineutrinos are right handed) they cannot be given mass through the Higgs mechanism if they are Dirac particles. Unlike other SM particles, neutrinos could be Majorana fermions and would be their own antiparticle. Many experiments are trying to observe neutrinoless double β decay, which would be a smoking gun signature of Majorana neutrinos. If it is observed neutrinos would explicitly violate lepton number (see [12] for more detail).

The Seesaw mechanism is the most popular theory that explains the smallness of the neutrino masses. Presented is a toy model where a heavy Majorana particle is added to the SM neutrino mass matrix

$$\mathbf{M} = \begin{pmatrix} 0 & xv \\ xv & M \end{pmatrix} \tag{19}$$

where M is the Majorana mass of the new particle, v is the vacuum expectation value of the Higgs field (measured at the LHC to be 246 GeV) and x is the mixing parameter between the two neutrinos. The small eigenvalue associated with the SM neutrinos would then be

$$m_{\text{small}} = \frac{1}{2} \left(M - \sqrt{M^2 + 4xv^2} \right)$$
 (20)

which goes as $(xv)^2/M$ for $M \gg xv$, making the SM neutrinos lighter for a heavier Majorana particle.

The Inverse Seesaw Mechanism (ISSM) adds a pseudo-Dirac fermion to the SM with a Dirac mass M_D . This fermion is made of two other particles, with their own Majorana masses. In ISSM the SM neutrino masses are proportional to the Majorana masses of the new particles meaning that if these Majorana masses are small, lepton number is minimally violated [13].

This analysis seeks to extend work done by Dr. Seyda Ipek and Cem Ayber on two theories combining ISSM and Supersymmetry adding two, and then four new SUSY particles in an ISSM scenario [14, 15]. These particles could be produced at a messenger scale $\Lambda_M \sim \mathcal{O}(100-1000\text{TeV})$. This range accommodates

the neutrino oscillation observables in the two models presented and previous searches of lepton flavour violation at lower energy.

The first model [14] adds two particles, the bino and singlino with Majorana masses $m_{\bar{B}}$ and m_S . These form a psudeo-Dirac particle known as the "bi ν o" with a Dirac mass M_D . The matrix describing the mass interactions in the $\{\nu_e, \nu_\mu, \nu_\tau, \bar{B}, S\}$ basis takes the form

$$\mathbf{M} \sim \begin{pmatrix} \mathbf{0}_{3\times3} & \mathbf{Y}v & \mathbf{G}v \\ \mathbf{Y}^T v & m_{\bar{B}} & M_D \\ \mathbf{G}^T v & M_D & m_S \end{pmatrix}, \ \mathbf{Y} = \frac{M_D}{\Lambda_M} \mathbf{b}, \ \mathbf{G} = \frac{m_{3/2}}{\Lambda_M} \mathbf{s}$$
(21)

where $m_{3/2}$ is the gravitino mass (another SUSY particle). The **Y** and **G** vectors describe the mixing of the bino and singlino with the SM particles and depend on two unit vectors **b** and **s**. The Majorana masses of the bino and singlino and gravitino are orders of magnitude smaller than Dirac mass

$$m_{\bar{B}} \sim m_S \sim m_{3/2} \sim \mathcal{O}(\text{keV}) \ll M_D \sim \mathcal{O}(\text{GeV} - \text{TeV})$$
 (22)

When finding the eigenvalues of equation 21, one mass will necessarily be zero (m_1) in the normal hierarchy). From the observed mass squared differences of the SM neutrinos

$$\mathbf{b} \cdot \mathbf{s} = \rho \simeq 0.7 \tag{23}$$

The components of the two vectors are found from the PMNS matrix elements and ρ with $i = e, \mu, \tau$

$$\mathbf{b} = \frac{1}{\sqrt{2}} \left(\sqrt{1+\rho} \ U_{i3}^* + \sqrt{1+\rho} \ U_{i2}^* \right) = \begin{pmatrix} 0.35 \\ 0.85 \\ 0.39 \end{pmatrix}$$

$$\mathbf{s} = \frac{1}{\sqrt{2}} \left(\sqrt{1+\rho} \ U_{i3}^* - \sqrt{1+\rho} \ U_{i2}^* \right) = \begin{pmatrix} -0.06 \\ 0.44 \\ 0.89 \end{pmatrix}$$
(24)

$$m_{2,3} = \frac{m_{3/2}v^2}{\Lambda_M^2}(1 \mp \rho) \tag{25}$$

The scenario with four SUSY particles [15] adds the wino and tripletino particles forming a second psudeo-Dirac particle, the "wi ν o". Notably this scenario permits three non-zero mass states for the SM neutrinos. The mass matrix in this theory is

$$\mathbf{M} = \begin{pmatrix} \mathbf{0}_{3\times3} & \mathbf{Y}_{\tilde{B}}v & \mathbf{Y}_{\tilde{W}}v & \mathbf{G}_{S}v & \mathbf{G}_{T}v \\ \mathbf{Y}_{\tilde{B}}^{T}v & m_{\tilde{B}} & 0 & M_{\tilde{B}} & 0 \\ \mathbf{Y}_{\tilde{W}}^{T}v & 0 & m_{\tilde{W}} & 0 & M_{\tilde{W}} \\ \mathbf{G}_{S}^{T}v & M_{\tilde{B}} & 0 & m_{S} & 0 \\ \mathbf{H}_{T}^{T}v & 0 & M_{\tilde{W}} & 0 & m_{T} \end{pmatrix}, \quad \mathbf{Y}_{\tilde{B}} = \frac{M_{\tilde{B}}}{\Lambda_{M}}\mathbf{b} \quad \mathbf{Y}_{\tilde{W}} = \frac{M_{\tilde{W}}}{\Lambda_{M}}\mathbf{w}$$

$$(26)$$

 $M_{\tilde{B}}$ and $M_{\tilde{W}}$ are the Dirac masses of the pseudo-Dirac particles and $m_{\tilde{W}}$ and m_T are the Majorana masses of the wino and tripletino, $\mathbf{Y}_{\tilde{B}}$, $\mathbf{Y}_{\tilde{W}}$, \mathbf{G}_S , \mathbf{G}_T are the SM interaction terms and each depends on one unit vector \mathbf{b} , \mathbf{w} , \mathbf{s} , \mathbf{t} . This matrix is not easily analytically solvable. In the scenario where $\mathbf{s} = \mathbf{t} = 0$ it returns the solutions of the 5-by-5 matrix, with $\mathbf{Y}_{\tilde{\mathbf{W}}} \to \mathbf{G}$ (eqn. 24)[15].

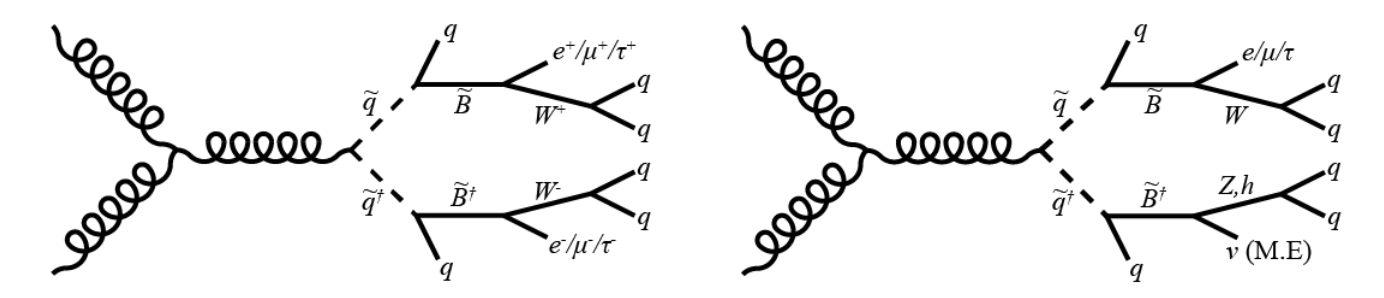


Figure 3: Decay structures of the bino into Standard model particles. \tilde{q} are squarks (supersymmetric quarks), W^+, W^-, Z^0 are the electroweak bosons and h is the Higgs boson. The decay products can be leptons, jets (quarks) or neutrinos (missing energy not collected by the LHC detectors).

Most analysis looks for unit vectors such that diagonalizing the mass matrices with the PMNS matrix returns SM neutrino mass states matching the mass constraints. The unit vectors characterize the decay structure of the new particles into SM particles which may be seen in the Large Hadron Collider (LHC) or future collider experiments. There are three ways for the bino (or wino if it happens to be lighter) to decay: $\tilde{B} \to W^{\pm} l^{\mp}$, $\tilde{B} \to Z\nu$ and $\tilde{B} \to h\nu$ (fig. 3). For many decays observed at the LHC, the ratio of the resulting final states $ee: \mu\mu$ and $e\nu: \mu\nu$ can be tested against the theoretical branching ratios given by unit vector elements as follows

$$\begin{pmatrix} |b_1|^2 \\ |b_2|^2 \\ |b_3|^2 \end{pmatrix} = \text{B.R.} \begin{pmatrix} e \\ \mu \\ \tau \end{pmatrix}$$
 (27)

2 Analysis

2.1 5-by-5 Matrix

The majority of the numerical analysis was performed in MATLAB due to its ability to work efficiently with vectors and matrices.

Initial analysis was performed on the 5-by-5 mass matrix since it already had and analytical solution, making it a good test case to develop numerical techniques. Since the diagonal Majorana mass terms were many orders of magnitude smaller than the Dirac mass terms, they could be set to zero with little effect on the diagonalization results (eqn. 28, based on eqn. 21).

$$\mathbf{M} \sim \begin{pmatrix} \mathbf{0}_{3\times3} & \mathbf{Y}v & \mathbf{G}v \\ \mathbf{Y}^T v & 0 & M_D \\ \mathbf{G}^T v & M_D & 0 \end{pmatrix}$$
 (28)

The other values were set as suggested by [14].

$$\Lambda_M \approx 100 \, {\rm TeV}$$

$$M_D \approx 1 \, {\rm TeV}$$

$$m_{3/2} \approx 10 \, {\rm keV}$$
(29)

The eigenvalues of \mathbf{M} returned the neutrino mass eigenstates. There were two TeV scale eigenstates for the Dirac masses of the bi ν o and antibi ν o, one zero mass eigenstate, and two with a magnitude between

0.001-0.1 eV. The eigenvectors of the light neutrino masses should form the PMNS matrix (i.e. the PMNS matrix should diagonalize upper 3-by-3 part of **M**).

2.1.1 General Techniques

The main variables being changed were the unit vectors **b** and **s**. It was important that these were being sampled from a uniform distribution over a sphere. However defining a sample distribution based on uniform values of θ and φ would lead to high anisotropy between the poles and the equator. The algorithm outlined by Gonzalez [16] was used to uniformly tile a sphere with points, creating an isotropic unit vector distribution.

MATLAB supports 3D matrices (rows, columns, pages) and can perform operations much more quickly on a single, paged matrix than iterating over the same number of 2D matrices with a for-loop. Analyzing samples this way uses considerably more RAM but was able to reduce computation time by well over a factor of 10 for very large scans.

Using the eig() function (or pageeig() for paged matrices) returns the eigenvalues and eigenvectors of M (eqn. 28). Diagonalizing the matrix was typically the most taxing operation of the algorithm; reducing the number of times eig() was called greatly improved efficiency.

A custom data type "float-with-error" (float_w_err) was created to represent a number with an associated uncertainty. It stores the central value and the upper and lower errors. By redefining the behavior of the eq() function for this data type, it is possible to check if a normal number falls within the bounds of a float-with-error using an equality statement. This method is more intuitive, clearer to read, and simpler to write than using greater- and less-than statements directly in the code. Additionally, making the errors larger for initial, sparse scans was much easier using this technique as the uncertainty was stored separately from the central value.

2.1.2 Finding the PMNS Matrix

The first scans over the possible **b** and **s** vectors focused on finding the correct PMNS matrix and looked at all possible combinations of vectors on the unit sphere. This algorithm required N^2 matrices to be checked so only a very sparse scan was possible. To compensate for this reduction, the uncertainty on individual PMNS matrix elements was set to an increased, uniform value. After finding some solutions it was noticed that if (\mathbf{b}, \mathbf{s}) was a solution returning the correct PMNS matrix, (\mathbf{s}, \mathbf{b}) and $(-\mathbf{b}, -\mathbf{s})$ were ones as well. Thus, the sample distribution of points could be restricted to one hemisphere and number of combinations being checked could be reduced to (N choose 2)+N (less than N^2 , but still including combinations where $\mathbf{b} = \mathbf{s}$) (fig. 4).

By further restricting the sampled points to only the slices seen on the two spheres in figure 4, the density could be increased and solutions that fit the actual PMNS matrix error bounds (eqn. 18) could be found.

2.1.3 Mass Difference Restrictions

The first step in including the masses was to verify the findings of the analytical result: The mass eigenvalues had no dependence on M_D and a linear dependence on $m_{3/2}$ (fig. 5). The PMNS solutions were independent of the two parameters.

From the analytical solution, it was known that the mass difference imposed a relation of $\mathbf{b} \cdot \mathbf{s} \approx 0.7$ between the two unit vectors. This was verified by choosing a single point for \mathbf{b} and then seeing which

PMNS Only Uniformly Padded Error Scan (U $_{ij} \pm 0.02$)

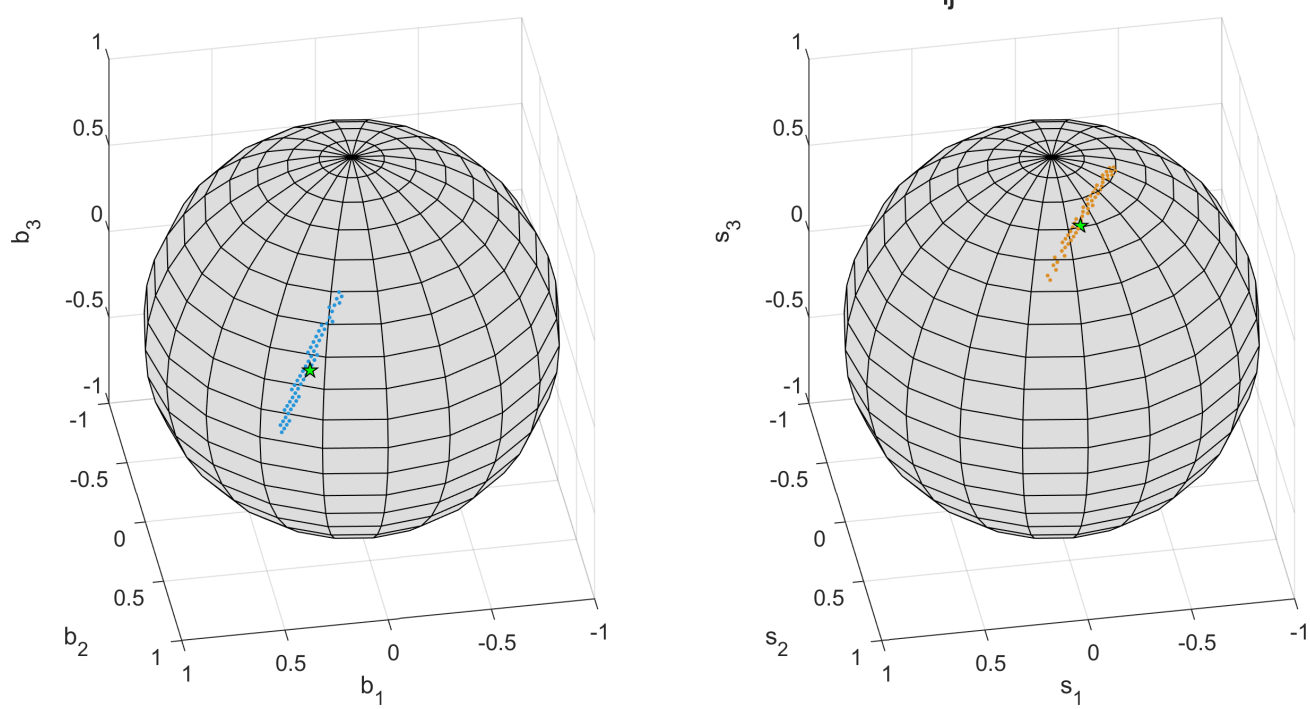


Figure 4: Unit sphere regions for **b** and **s** that return correct PMNS matrix. Points were restricted to the hemisphere $y_2 > 1$ and only unique combinations were looked at. Padding of ± 0.02 has been taken as the "error" for every element of the known PMNS matrix to admit more solutions during this exploratory scan. The red stars show the expected values of **b** and **s** taken from [14].

points for \mathbf{s} would return the correct mass eigenvalues. The pattern of points that were admitted formed a ring on the unit sphere around the point \mathbf{b} and had an average dot product of 0.7055.

This restriction was first applied loosely so an ideal value for the gravitino mass could be set. Looking at mass histograms for $|\Delta m_{21}|^2$, and $|\Delta m_{31}|^2$, setting $m_{3/2} \simeq 4.85 \,\mathrm{keV}$ maximized the number of **b** and **s** returning correct mass differences (fig. 6).

2.1.4 Solution of the 5x5 Matrix

A final, very dense scan was performed with points sampled from near the PMNS solutions and combinations were excluded based on their dot products. This could be done before the taxing diagonalization procedure, speeding up analysis. The solutions for the **b** and **s** vectors satisfied the errors on the PMNS matrix and those on the mass squared differences (eqns. 18, 17, fig. 7). The final values below are the mean of those solutions:

$$\mathbf{b} = \begin{pmatrix} 0.35 \\ 0.83 \\ 0.44 \end{pmatrix}, \ \mathbf{s} = \begin{pmatrix} -0.07 \\ 0.40 \\ 0.91 \end{pmatrix}, \ m_1 = 0 \,\text{eV}, \ m_2 = 0.0089 \,\text{eV}, \ m_3 = 0.0498 \,\text{eV}$$
 (30)

These results are close to those of the analytical solution for the 5-by-5 matrix (eqn. 24). One note is that the mass eigenstates still depend on the choice of the gravitino mass $(m_{3/2})$ which can vary slightly and admit some valid solutions.

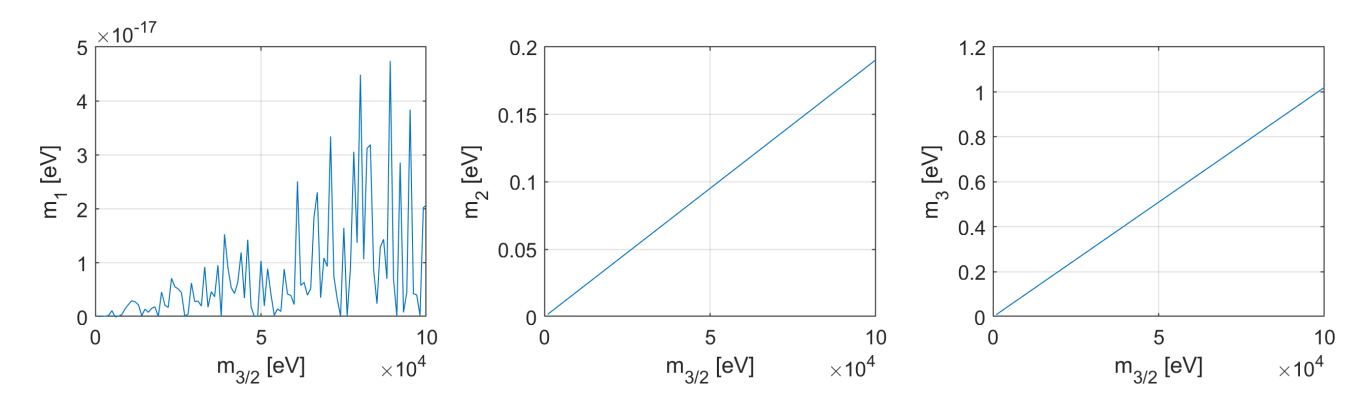


Figure 5: Mass eigenstates of **M** and their dependence on gravitino mass (**b** and **s** fixed to an arbitrary PMNS solution [fig. 4]). m_1 is zero (with some numerical fluctuations), m_2 and m_3 depend linearly on $m_{3/2}$.

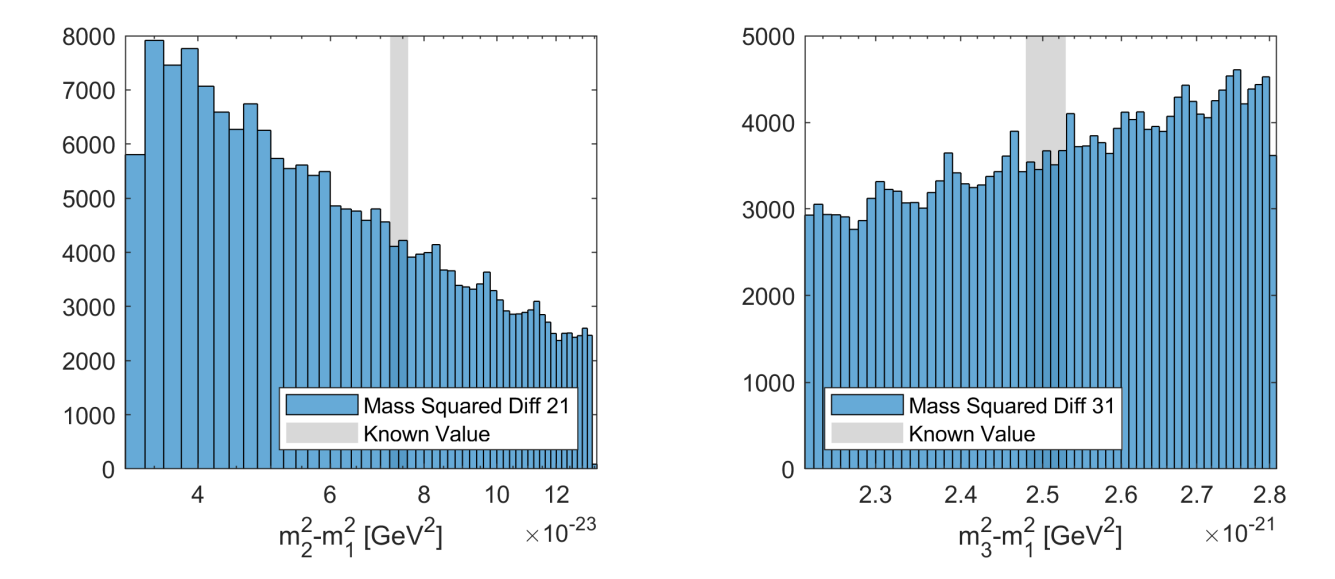


Figure 6: Histogram of $|\Delta m_{21}|^2$, and $|\Delta m_{31}|^2$ from a 2d scan over **b** and **s** where $\mathbf{b} \cdot \mathbf{s} = 0.7 \pm 0.1$ and $m_{3/2} \simeq 4.85 \,\text{keV}$.

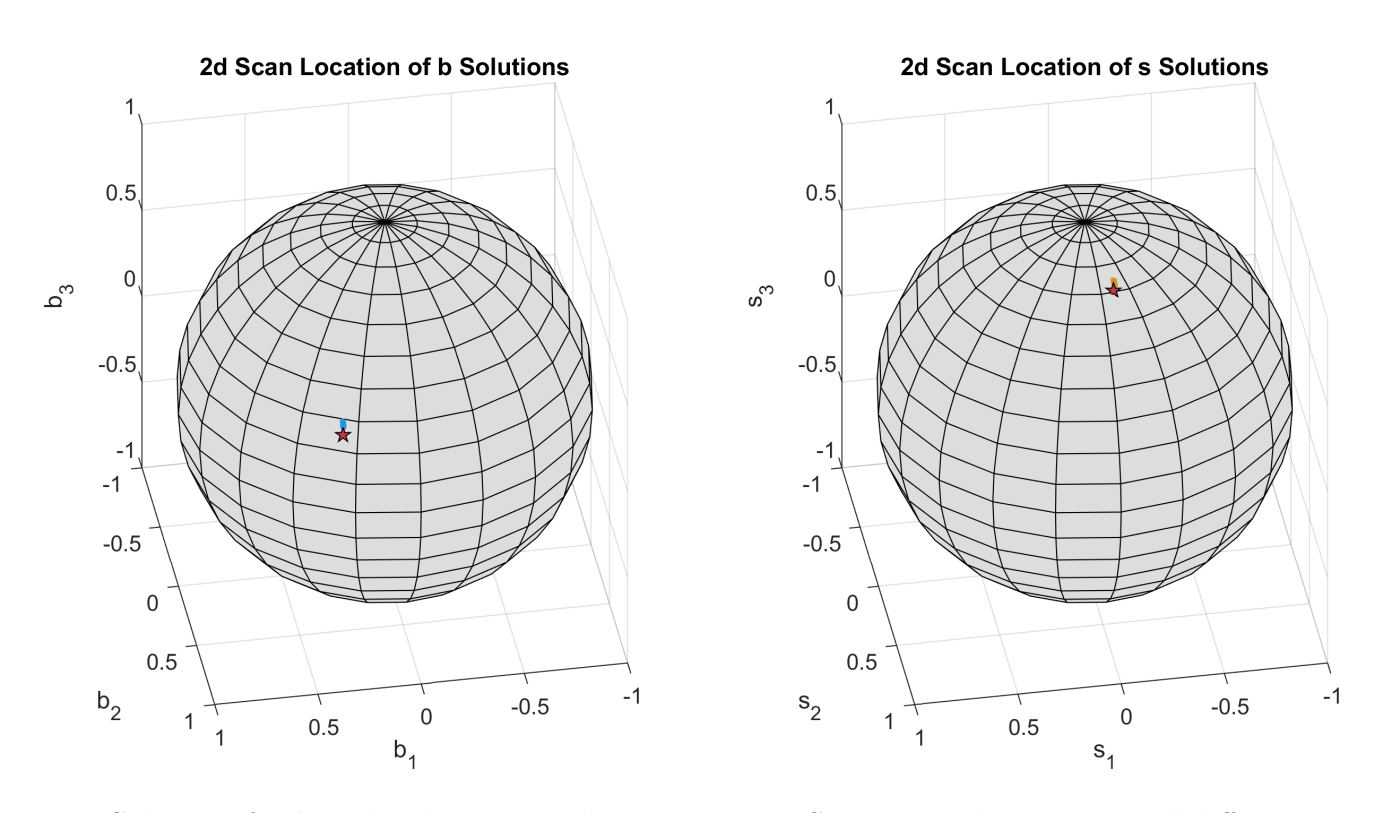


Figure 7: Solutions for $\bf b$ and $\bf s$ that return the correct PMNS matrix and mass squared differences. The red stars represent the expected locations of the vectors.

2.2 The 7x7 Mass Matrix

As with the 5-by-5 equation, the Majorana masses on the diagonal of the 7-by-7 mass matrix were set to zero (eqn. 26). Unlike the 5-by-5 matrix, there are scenarios where all 3 of the SM neutrino masses are non-zero.

$$\mathbf{M} = \begin{pmatrix} \mathbf{0}_{3\times3} & \mathbf{Y}_{\tilde{B}}v & \mathbf{Y}_{\tilde{W}}v & \mathbf{G}_{S}v & \mathbf{G}_{T}v \\ \mathbf{Y}_{\tilde{B}}^{T}v & 0 & 0 & M_{D} & 0 \\ \mathbf{Y}_{\tilde{W}}^{T}v & 0 & 0 & 0 & M_{D} \\ \mathbf{G}_{S}^{T}v & M_{D} & 0 & 0 & 0 \\ \mathbf{H}_{T}^{T}v & 0 & M_{D} & 0 & 0 \end{pmatrix}$$
(31)

Searches for lepton flavour violating $\mu \to e + \gamma$ and $\mu \to e$ conversion around nuclei put a lower bound on the messenger scale (figure 1 in [15]). To keep the SM neutrino mass states on the order of eV, the gravitino mass was increased to the MeV scale to keep $m_{3/2}/\Lambda_M^2$ the same.

$$\Lambda_M \sim 1000 \, {\rm TeV}$$

$$M_D \approx 1 \, {\rm TeV}$$

$$m_{3/2} \sim 1 \, {\rm MeV}$$
(32)

The first test performed was to verify the analytic solution from [15] in the case that $\mathbf{w} = \mathbf{t} = 0$. The numerical result agrees with the analytical result for this special case, where \mathbf{b} and \mathbf{s} take on the 5-by-5 results with a massless eigenvalue (eqn. 30):

$$\mathbf{b} = \begin{pmatrix} 0.35 \\ 0.83 \\ 0.44 \end{pmatrix}, \ \mathbf{s} = \begin{pmatrix} -0.07 \\ 0.40 \\ 0.91 \end{pmatrix}$$
 (33)

Scanning over sets where more than two vectors were free to vary on the unit sphere proved computationally taxing. It was not feasible at a high enough point density to admit solutions. If **b** and **s** (or **w** and **t**) were set to the 5-by-5 result and one other left to vary, many solutions were found indicating that there was little dependence on the free vector (explained later by the partial analytical solution). If at least one vector was set to be zero, there would be one zero mass eigenvalue. With four non-zero vectors there were three non-zero mass eigenvalues but there was no simple dependence between vector values and the mass eigenvalue results such as the dot product in the 5-by-5 case.

2.2.1 The O Matrix

It was clear that the 7-by-7 system would be very under-constrained as there were 10 parameters (2 × 4 parameters per unit vector, Λ_M and $m_{3/2}$) to only five constraints (three mixing angles and two mass-squared differences). From initial testing, it was determined that the 7-by-7 case with all four vectors being non-zero could not be solved (in a reasonable time) with only numerical methods. It was decided to attempt a hybrid analytical-numerical solution, with the analytical method providing a more efficient framework to finding valid 7-by-7 mass matrices (fig. 8). The intuition was that a partial analytical solution would provide some domain restrictions, like the dot product in the 5-by-5 matrix.

Assuming that the diagonal terms in M (eqn. 31) are zero, the $c^{d=5}$ coefficient of the Weinberg operator is [13]

$$c^{d=5} = \frac{m_{3/2}}{\Lambda_M^2} \left(\mathbf{b} \ \mathbf{s}^T + \mathbf{s} \ \mathbf{b}^T + \mathbf{w} \ \mathbf{t}^T + \mathbf{t} \ \mathbf{w}^T \right) = \frac{m_{3/2}}{\Lambda_M^2} \mathbf{O}$$
 (34)

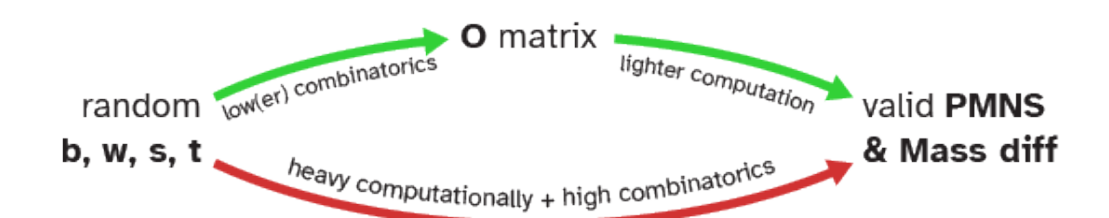


Figure 8: A flowchart explaining benefits of the intermediate **O** matrix step on computations and combinatorics. The first step is to find the set of **O** matrices that return the correct PMNS and mass differences upon diagonalization for a specific ratio of $m_{3/2}/\Lambda_M^2$. The second is then to find a combination of **bwst** vectors mapping to one of those valid matrices.

where **O** is a 3-by-3 symmetric matrix

$$\begin{pmatrix}
O_{11} & O_{12} & O_{13} \\
O_{12} & O_{22} & O_{23} \\
O_{13} & O_{23} & O_{33}
\end{pmatrix}$$
(35)

with elements

$$O_{11} = 2(b_1s_1 + w_1t_1) O_{12} = b_1s_2 + s_1b_2 + w_1t_2 + t_1w_2 O_{22} = 2(b_2s_2 + w_2t_2) O_{13} = b_1s_3 + s_1b_3 + w_1t_3 + t_1w_3 O_{33} = 2(b_3s_3 + w_3t_3) O_{23} = b_2s_3 + s_2b_3 + w_2t_3 + t_2w_3$$

$$(36)$$

This matrix O can then be diagonalized by the PMNS matrix to return SM neutrino mass states

$$\frac{m_{3/2}v^2}{\Lambda_M^2}U_{\text{PMNS}}^{\dagger} \mathbf{O} U_{\text{PMNS}} = \mathbf{O}_d, \ \mathbf{O}_d = \begin{pmatrix} m_1 & 0 & 0 \\ 0 & m_2 & 0 \\ 0 & 0 & m_3 \end{pmatrix}$$
(37)

As a corollary, if a symmetric matrix **O** can be found such that its eigenvectors form the PMNS matrix, and whose eigenvalues follow the allowed mass-squared differences, any set of **bwst** vectors that create **O** as per equation 34 would also solve the 7-by-7 matrix (fig. 8). This subset of "valid **O** matrices" is what is provided as an intermediate step in the diagonalization process. The computational step of checking the eigenvectors and eigenvalues of **O** is much less intensive compared to that for the 7-by-7 matrix as it is only a 3x3 matrix with entries of order 1.

Using the known PMNS matrix, equation 37 can be used to rewrite **O** to remove some of the linear dependence among its terms. The zero elements in \mathbf{O}_d can be used to write the $O_{i\neq i}$ elements as a function of O_{ii} (i=1,2,3).

$$\mathbf{O} = \begin{pmatrix} O_{11} & 0.72O_{11} - 5.1O_{22} + 4.4O_{33} & -1.3O_{11} + 6.3O_{22} - 4.9O_{33} \\ 0.72O_{11} - 5.1O_{22} + 4.4O_{33} & O_{22} & -2.3O_{11} + 7.5O_{22} - 5.2O_{33} \\ -1.3O_{11} + 6.3O_{22} - 4.9O_{33} & -2.3O_{11} + 7.5O_{22} - 5.2O_{33} & O_{33} \end{pmatrix}$$
(38)

Trying to incorporate the mass squared differences to rewrite **O** was too unwieldy as they are non-linear for m_1 , m_2 , m_3 .

The mass eigenstates from equation 37 can be rewritten in terms of the diagonal elements as well

$$\frac{\Lambda_M^2}{m_{3/2}v^2}m_1 = 0.11 O_{11} + 5.2 O_{22} - 4.3 O_{33}$$

$$\frac{\Lambda_M^2}{m_{3/2}v^2}m_2 = 3.3 O_{11} - 12.0 O_{22} + 10.0 O_{33}$$

$$\frac{\Lambda_M^2}{m_{3/2}v^2}m_3 = 8.1 O_{22} - 2.4 O_{11} - 4.7 O_{33}$$
(39)

The limits of the space spanned by $O_{ii} \in \mathbb{R}^3$ depends on the **bwst** vectors. The shape of this subspace was found by plotting **O** matrices generated from random sets of **bwst** vectors and it reveals that the diagonal elements O_{ii} must have a one-norm less than or equal to 4, creating an outer boundary that was used when searching for valid **O** matrices.

$$|O_{11}| + |O_{22}| + |O_{33}| = ||O_{ii}||_1 \le 4$$

The off-diagonal terms around bounded within $||O_{i\neq j}|| \leq 2$.

A 3D scan using the diagonal entries of **O** within the regions of $||O_{ii}||_1 \le 4$ was performed to find the set of valid solutions for O_{ii} within the uncertainty on the PMNS matrix and the mass differences. Scans were performed three times, for different ratios of $m_{3/2}/\Lambda_M^2$: gravitino masses of 500 keV, 1 MeV and 2 MeV were used with $\Lambda_M = 1000$ TeV held constant throughout.

The scans were preformed in two steps. The first was a coarse scan over the entire space of O_{ii} that admitted a small number of solutions (blue points in fig. 10). A Bézier curve was visually fit to those points to define a "spine" for the second scan which was performed in a radius around that curve. The second scan provided a dense set of solutions for valid O matrices (fig. 11).

The set of **O** that returned correct PMNS matrices upon diagonalization was independent of the gravitino mass and messenger scale which is expected from equation 37. The diagonalization produced a single set of valid mass eigenvalues for all gravitino masses (fig. 12). As the gravitino mass was increased, the elements of valid **O** were linearly scaled towards the origin $O_{ij} \propto \Lambda_M^2/m_{3/2}$ (fig. 11).

2.2.2 Finding bwst Vectors

Finding **bwst** vectors mapping to valid **O** matrices is still a difficult problem. The space of matrices that can be made from **bwst** vectors as per equation 34 has a volume of

$$(||O_{ij}||_1 \le 4) \times (||O_{i \ne j} \le 2||) = \frac{4}{3}4^3 \times \frac{4}{3}\pi 2^3 \simeq 2860$$

There are **bwst** vectors can map to a number of **O** matricies equal to $n_O \simeq 2860 \times 10^{3r}$ (entries rounded to the r-th decimal place). Only a small subset of these matrices are valid **O**. For r = 1, $n_O \sim 10^6$. That is a reasonable number to scan over using random **bwst** combinations drawn from the unit sphere. In actuality, the distribution is not uniform, but for $10^7 - 10^8$ random **bwst** combinations, a few do lead to valid **O**.

When rounding the **O** matrices to $r \ge 2$, the number of possible O matrices is $n_o \sim 10^9$. This is too high to find the small number of valid **O** by drawing random **bwst** vectors from the entire unit sphere. The unit vector distributions are limited to a spherical cap of the unit sphere of radius θ centered on the

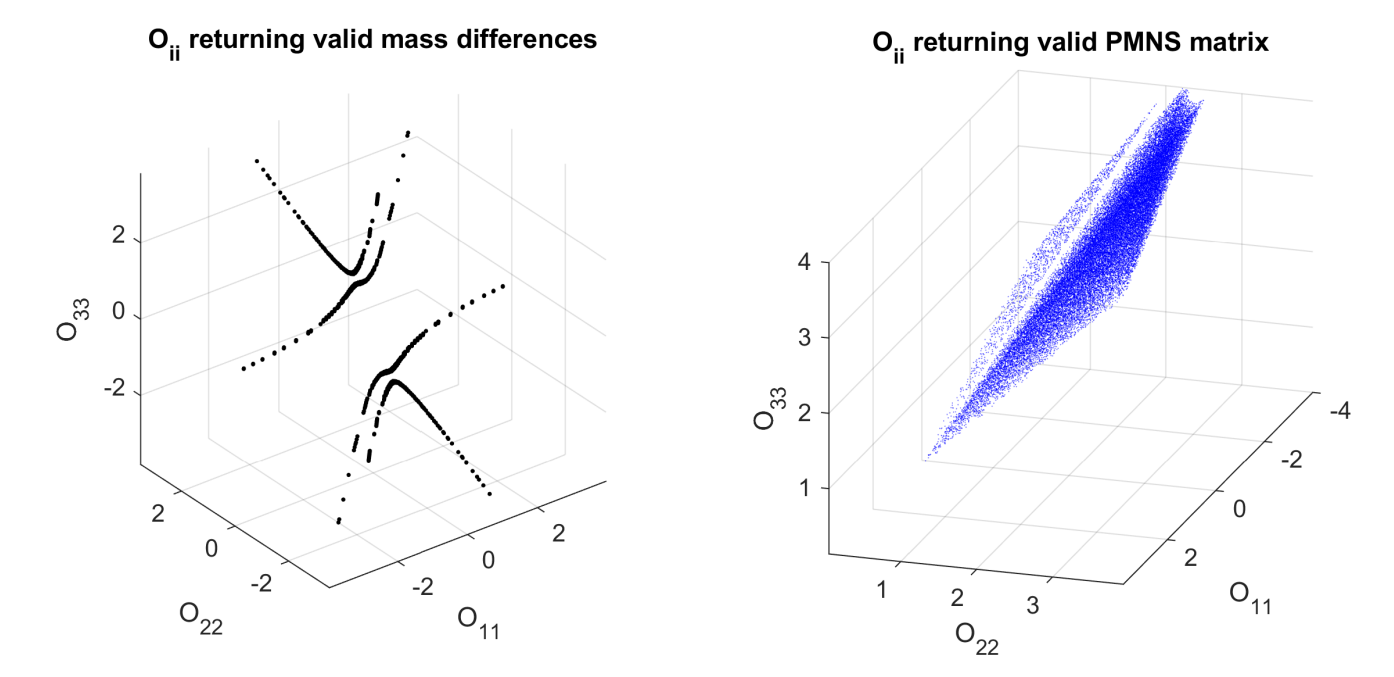


Figure 9: Left: Values for $||O_{ii}||$ that satisfy the mass differences (eqn. 39). Right: Points satisfying U_{PMNS} (1/100th of points shown)(eqn. 18, 38).

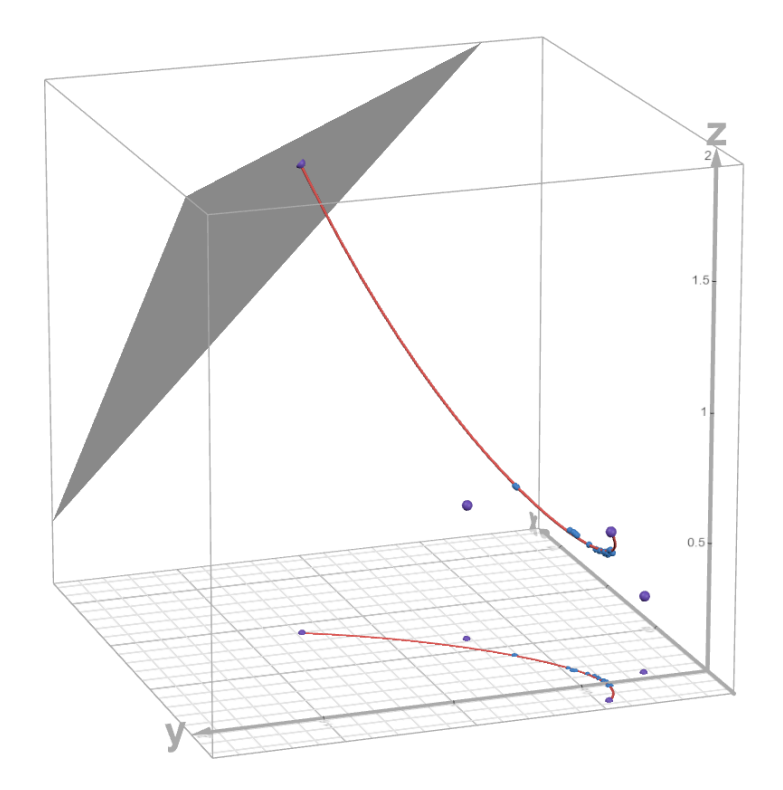


Figure 10: Visually fitting a cubic Bézier curve (control points marked in purple) to points along the intersection of the the graphs in figure 9 (small points in blue). The fourth Bézier control point lies on the surface defined by $||O_{ii}||_1 \le 4$ (grey plane). A copy of the graph has also been projected onto the x-y plane below. Made in Desmos 3D.

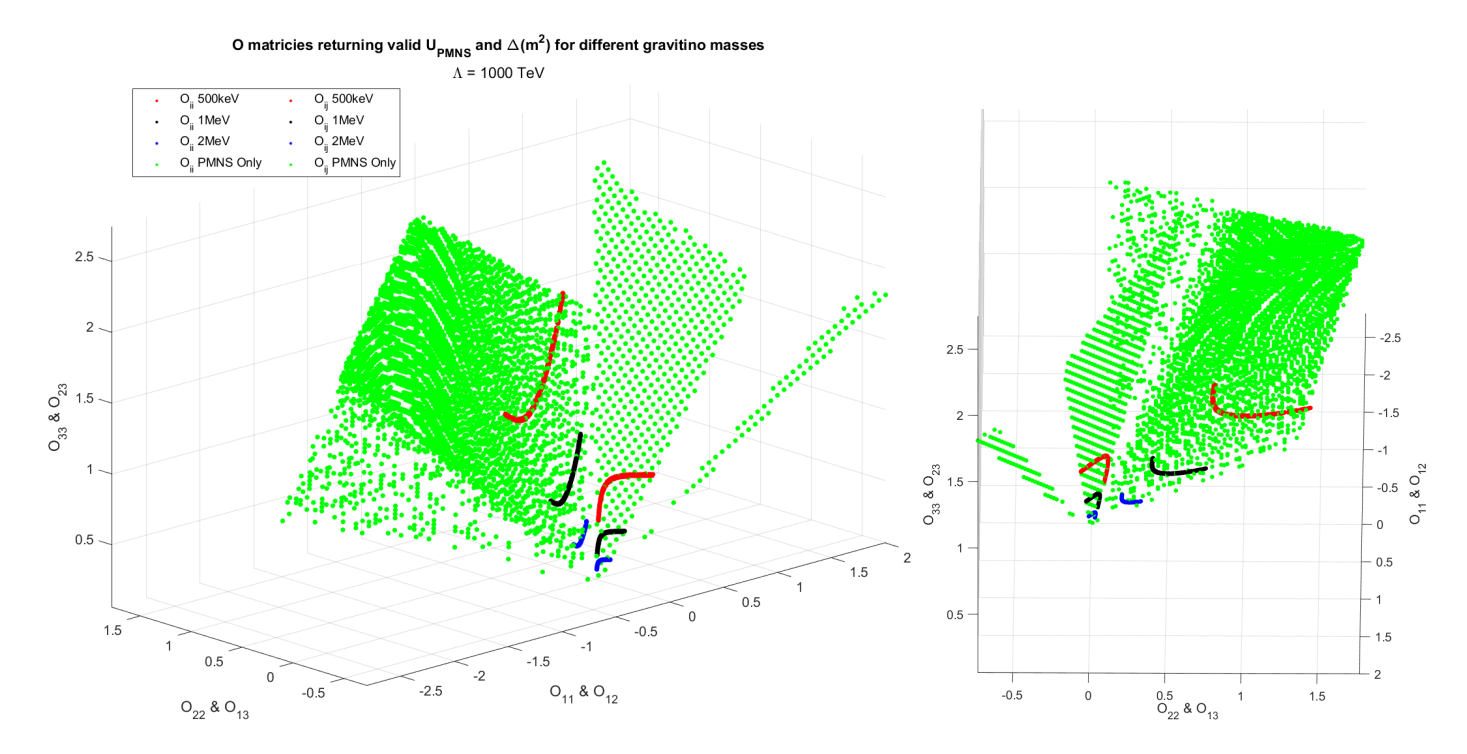


Figure 11: Two views of **O** matrix elements (diagonal, $||O_{ii}||$ and off-diagonal $||O_{i\neq j}||$) for various values of gravitino mass (red - 500 keV, black - 1 MeV, blue 2-MeV). The curves satisfy both the mixing parameters (eqn. 18, 38) and the maximum norm limit. The green points show the valid points only looking at the norm limit and U_{PMNS} , which are independent of gravitino mass.

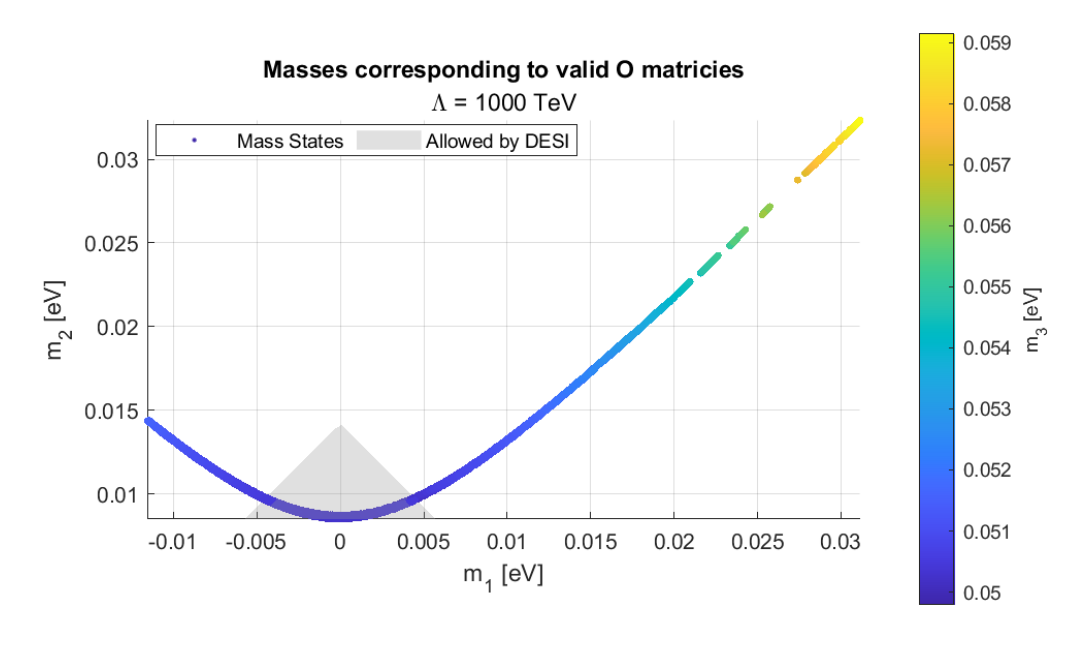


Figure 12: The set of valid neutrino mass eigenstates corresponding to all 3 curves in figure 11. Points within the grey region fall within the upper bound on the sum of neutrino masses found by the DESI collaboration of $\sum m_{\nu} < 0.064$ [10].

Table 1: **bwst** vectors that produce a valid **O** and 7-by-7 matrices with one massless SM neutrino $(m_1 \simeq 0)$ for various gravitino masses.

	b	\mathbf{w}	\mathbf{s}	${f t}$
	(0.64)	/ -0.43	(-0.29)	$\sqrt{-0.57}$
$m_{3/2} = 500 \text{ keV}$	0.34	-0.81	-0.71	-0.81
,	$\setminus -0.69$	(-0.40)	(-0.64)	$\setminus -0.14$
	(0.04)	(0.61)	0.73	(0.00)
$m_{3/2} = 1 \text{ MeV}$	0.62	0.15	0.46	-0.56
	(0.78 /	(-0.78)	$\left(\begin{array}{c} -0.51 \end{array}\right)$	-0.83

Table 2: **bwst** vectors that produce a valid **O** and 7x7 matrices with 3 massive SM neutrinos ($m_1 \neq 0$) for various gravitino masses.

	b	\mathbf{W}	\mathbf{S}	${f t}$
	(0.23 \	(-0.06)	(-0.14)	(-0.12)
$m_{3/2} = 500 \text{ keV}$	-0.77	-0.97	0.66	-0.93
,	$\setminus -0.60$	$\setminus -0.23$	$\setminus -0.74$	$\setminus -0.34$
	(0.75)	0.96	(0.66)	$\sqrt{-0.53}$
$m_{3/2} = 1 \text{ MeV}$	0.52	0.25	0.62	-0.48
	(0.41)	(-0.12)	(0.43)	-0.70

vector found for r = 1 (see **w** and **t** plots in fig. 13 with $\theta = 0.05$ rad). By "perturbing" the vectors found in the previous step in this way, it is possible to converge on **bwst** vectors creating a valid **O** matrix. This can be repeated for higher values of r, but it was found that r = 3 was sufficient to produce **bwst** vectors that lead to valid 7-by-7 matrices.

For cases where only a small subset of valid O matrices were being targeted (such as matrices with an eigenvalue close to zero), this method would still have difficulty converging. The chance of finding valid **bwst** vectors could be increased by changing the vector distribution caps on the fly. If a set of **bwst** vectors created an O matrix closer (in \mathbb{R}^6 euclidean distance) to the targeted O than the current vectors defining the caps, the caps would be recentered on the new vectors. This method found more solutions much faster as the distribution cap centers converged to the valid set of **bwst** vectors.

Once **bwst** vectors were found that matched a valid **O** matrix in the third decimal place, they could be verified in the 7-by-7 matrix (tbl. 1, 2). The techniques presented above; letting the vectors be "perturbed" in a cap, and shifting the center of the caps, worked well to find more **bwst** vectors that produced valid 7-by-7 matrices (fig. 13).

In all of these results, there was less of a constraint on the **w** and **t** vectors than the **b** and **s** ones (fig. 13). The **wt** vectors would have solutions in the entire space they could be perturbed in, whereas the **b** vector solution took on a narrower shape that extended to the edges of the perturbation region. The set of **bwst** vectors for a specific set of neutrino masses was not unique either (tbl. 1, row 1 and tbl. 3).

The technique used to shift the perturbation area also works in the 7-by-7 matrix to find solutions with slightly different parameters. The **bwst** vectors admitting solutions were recorded for incremental changes in different parameters such as $m_{3/2}$ or Λ_M , or to converge to specific mass eigenvalues.

Increasing the gravitino mass caused the mass eigenstates to grow heavier (fig. 14). This was more pronounced for eigenstates without a massless neutrino. The **b** and **s** vectors changed much more than

Table 3: Another set of **bwst** vectors that produce a valid **O** and 7-by-7 matrices with one massless SM neutrino $(m_1 \simeq 0)$ for $m_{3/2} = 500 \text{ keV}$

b	\mathbf{W}	\mathbf{s}	\mathbf{t}
(0.11)	(-0.51)	(0.70 \	(0.04)
0.73	-0.12	0.67	0.63
$\setminus 0.68$	\setminus 0.85	$\setminus 0.24$	$\setminus 0.78$

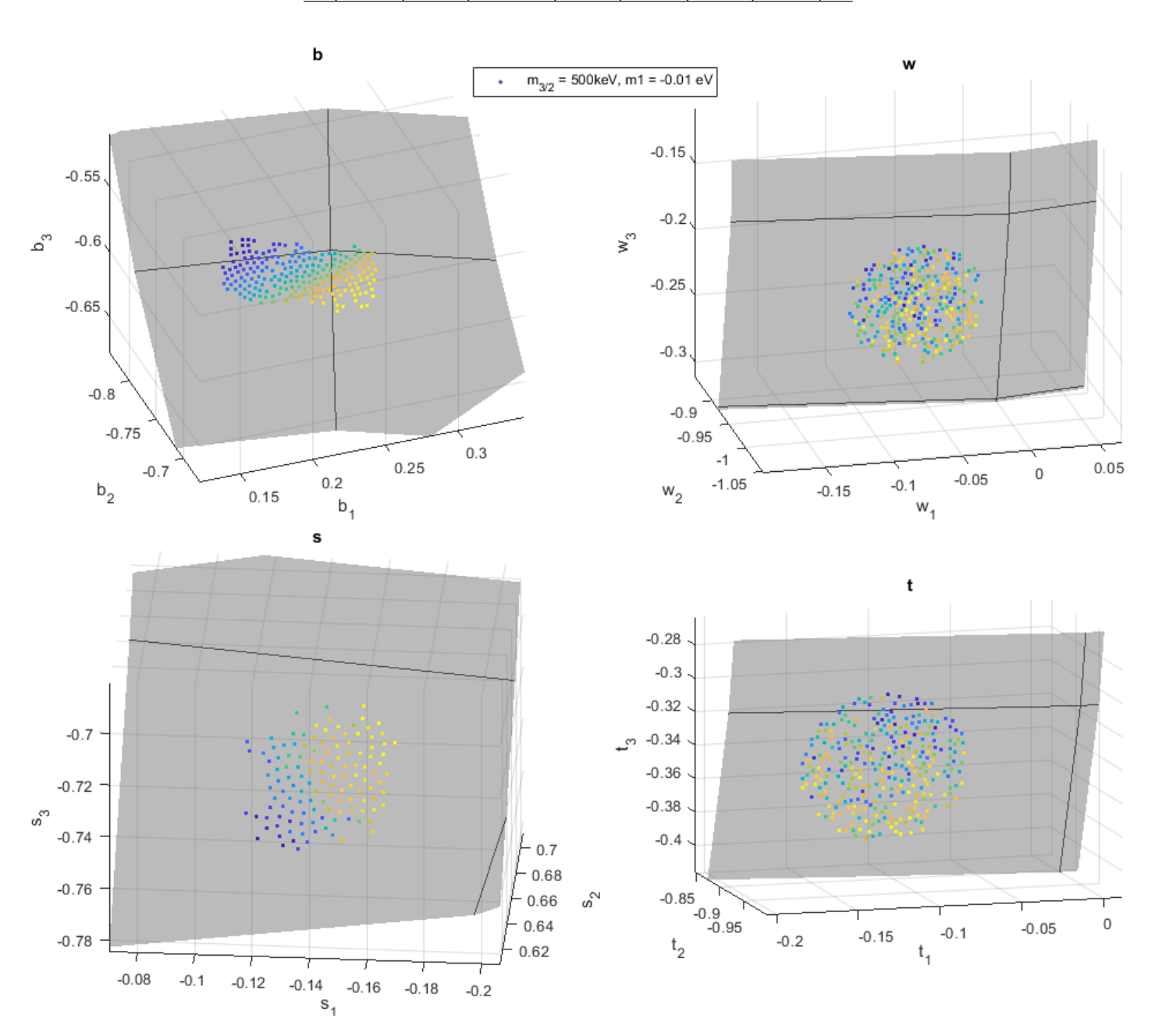


Figure 13: Valid **bwst** vectors for $m_{3/2} = 500$ keV and $m_1 \approx -0.01$ eV. Combinations of vectors within a spherical cap of $\theta = 0.05$ rad from the **bwst** vectors in table 2 (row 1) were verified. Sets of **bwst** vectors are grouped by colour and sorted by b_1 . The grey surface is a portion of the unit sphere.

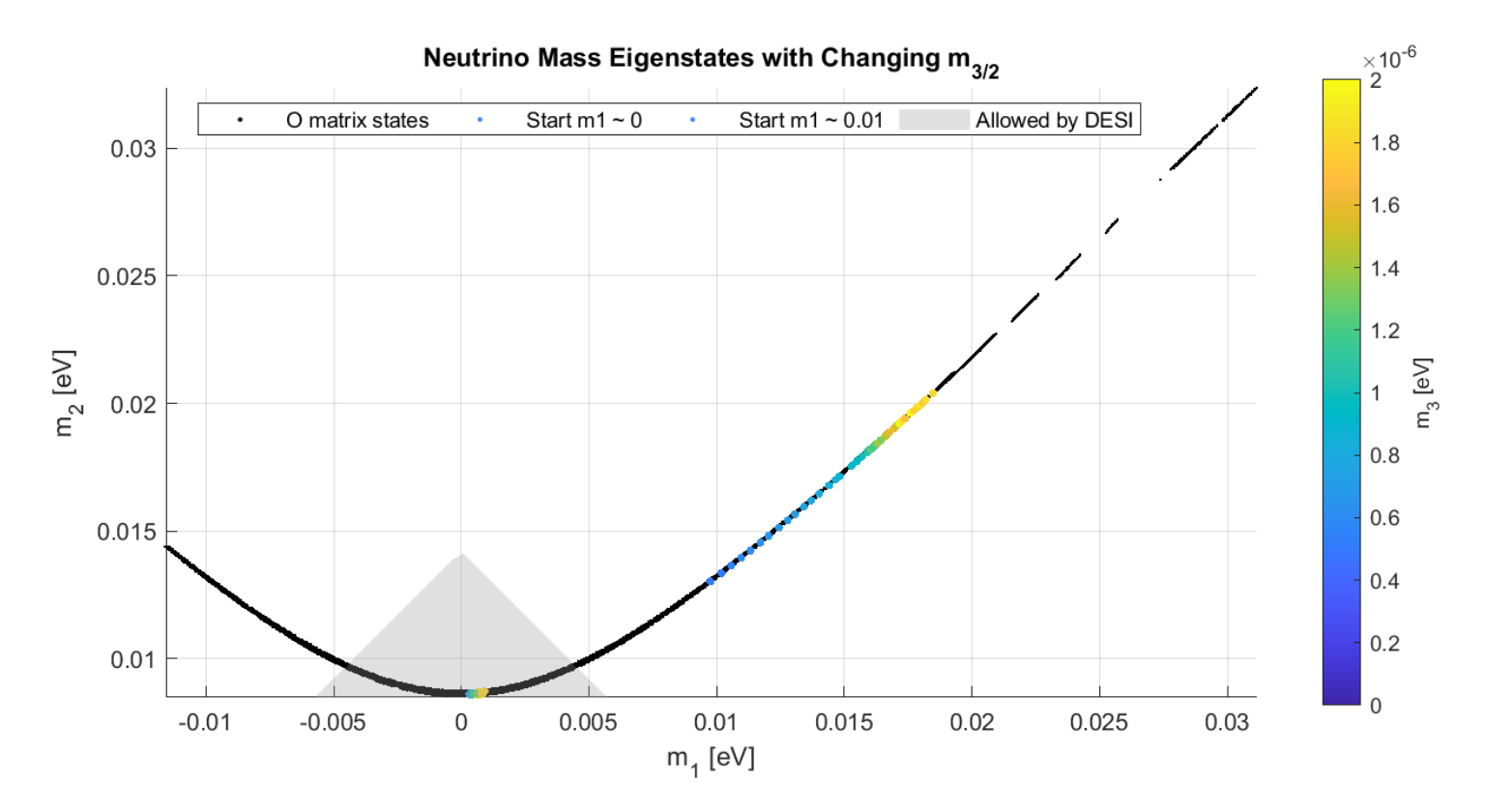


Figure 14: Changing mass eigenstates for incremental changes to gravitino mass. One track started with $m_1 \approx 0$ eV, the other with $m_1 \approx 0.01$ eV. Black points are the mass eigenstates shown in figure 12 for reference. Points within the grey region fall within the upper bound on the sum of neutrino masses found by the DESI collaboration of $\sum m_{\nu} < 0.064$ [10].

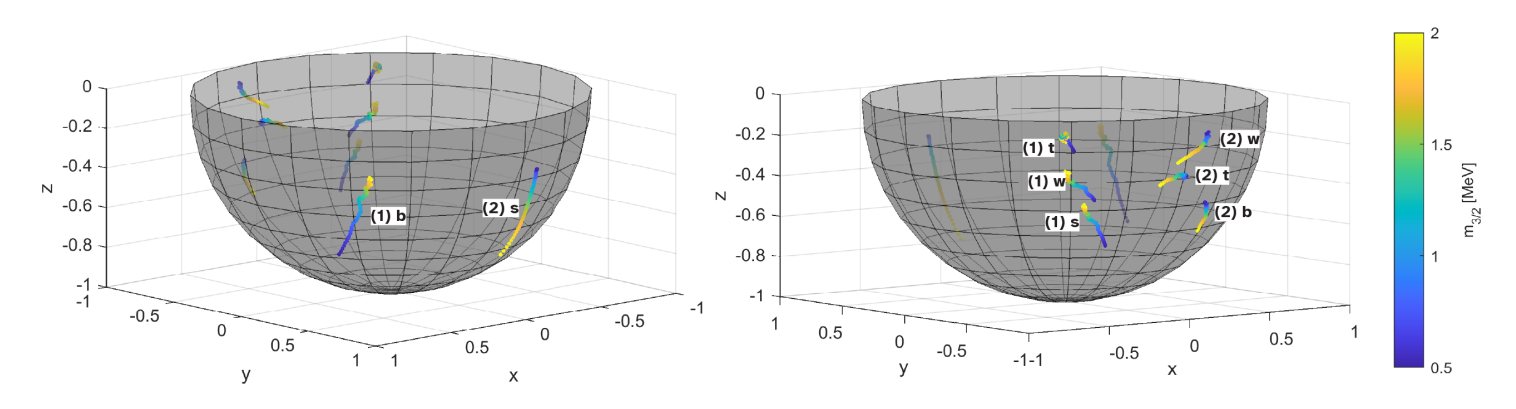


Figure 15: Changing of **bwst** vector solutions for incremental changes to gravitino mass, shown on a unit sphere. (1) starting with $m_1 \approx 0$ eV, (2) starting with $m_1 \approx 1$ eV (fig. 14).

the **w** or **t** ones as the gravitino mass increased (fig. 15). Increasing the messenger scale caused the mass states to scale in an inverse manner with them getting lighter and the same trends were seen in the **bwst** vectors.

3 Conclusion

The model investigated in this analysis explains the mass of the SM neutrinos by using the Inverse Seesaw Mechanism to add SUSY particles to the neutrino mass matrix. The mass matrices presented depend on unit vectors which characterize the decay structure of the SUSY particles to SM particles, the messenger scale and, the gravitino mass. Valid mass matrices can be diagonalized by the PMNS matrix and return SM neutrino mass states matching the mass squared differences and mass sum limit set by DESI [9, 8, 10].

This analysis used numerical methods in MATLAB to explore two theories: one adding two new particles, the bino and singlino (5-by-5 matrix case) and then adding two more particles, the wino and tripletino (7-by-7 matrix case). The 5-by-5 case is solvable analytically and requires that one SM neutrino be massless. The numerical result was verified the analytical solution. The 7-by-7 case is an underconstrained system with 10 free variables: four unit vectors (**b**, **w**, **s**, **t**), the messenger scale and the gravitino mass. There remain five constraints: the three mixing angles and two mass squared differences. Notably, the 7-by-7 case does not require one of the SM neutrinos to be massless but could not be solved analytically without major simplifications.

To solve the 7-by-7 mass matrix, a method was developed that could find sets of **bwst** vectors for specific SM mass states using a set of symmetric matrices **O** as an intermediate step. Sets of solutions were found for various gravitino masses and different eigenstates. Next, starting with a previous solution for the 7-by-7 matrix, the unit vectors could be perturbed repetitively to find **bwst** vectors for a precise mass eigenvalue, or to see how the **bwst** vectors were affected by changing the gravitino mass and messenger scale. It was found that the **b** and **s** unit vectors typically affect the solution much more than the **w** and **t** ones. When solutions were perturbed, **wt** took on a greater range of values and were less constrained. Moreover, while incrementally changing the gravitino mass, the **bs** vectors moved much more on the unit sphere than the **wt**.

It was discovered that there are multiple sets of **bwst** that produce the same neutrino mass states. In particular there is no "smoking gun" set of vectors that produced a massless neutrino. If there was, an observation of the specific branching ratio given by **b** for a potential bino/wino decay in a collider experiment could confirm a massless neutrino. If leptonic branching ratios in bino decays are measured in the LHC it would be possible to include them as a strong constraint in this model. Meanwhile, the solutions presented in this analysis can be used in MadGraph, a tool for simulating collider signals for Standard Model or Beyond Standard Model theories of particle physics. It is hoped that some of these solutions may lead to other interesting signatures that could be searched for at the Large Hadron Collider.

Low-energy/cosmological constraints continue to narrow the solution space further. The recent DESI publication on the upper limit on the sum of neutrino masses restricts the number of valid mass eigenstates significantly in the 7-by-7 model. There is a smaller band still which still includes the possibility of a massless SM neutrino. Results very recently released by the KATRIN experiment show that they have placed an upper limit of $m_{\nu} < 0.45$ eV on the heaviest neutrino mass with 90% confidence [11]. This limit is far above the DESI limit, but future results from KATRIN are expected to push it lower, possibly discovering the heaviest neutrino mass.

4 References

- ¹R. Davis, D. S. Harmer, and K. C. Hoffman, "Search for neutrinos from the sun", Phys. Rev. Lett. **20**, 1205–1209 (1968).
- ²D. Griffiths, *Introduction to elementary particles*, 2nd rev. ed. (Wiley-VCH, 2008), pp. 387–398.
- ³V. Gribov and B. Pontecorvo, "Neutrino astronomy and lepton charge", Physics Letters B **28**, 493–496 (1969).
- ⁴V. A. Rubakov and D. S. Gorbunov, *Introduction to the Theory of the Early Universe: Hot big bang theory* (World Scientific, Singapore, 2017).
- ⁵K. S. Hirata et al., "Observation of ⁸B solar neutrinos in the kamiokande-ii detector", Phys. Rev. Lett. **63**, 16–19 (1989).
- ⁶Q. R. Ahmad et al. (SNO Collaboration), "Direct evidence for neutrino flavor transformation from neutral-current interactions in the sudbury neutrino observatory", Phys. Rev. Lett. **89**, 011301 (2002).
- ⁷K. Eguchi et al., "First results from kamland: evidence for reactor antineutrino disappearance", Physical Review Letters **90**, 10.1103/physrevlett.90.021802 (2003).
- ⁸Wikipedia contributors, *Pontecorvo-maki-nakagawa-sakata matrix Wikipedia*, the free encyclopedia, [Online; accessed 20-August-2024], 2024.
- ⁹I. Esteban, M. Gonzalez-Garcia, M. Maltoni, T. Schwetz, and A. Zhou, "The fate of hints: updated global analysis of three-flavor neutrino oscillations", Journal of High Energy Physics **2020**, 10.1007/jhep09(2020)178 (2020).
- ¹⁰D. Collaboration et al., Desi dr2 results ii: measurements of baryon acoustic oscillations and cosmological constraints, 2025.
- $^{11}\mathrm{M}.$ Aker et al., Direct neutrino-mass measurement based on 259 days of katrin data, 2024.
- ¹²J. J. Gómez-Cadenas, J. Martín-Albo, J. Menéndez, M. Mezzetto, F. Monrabal, and M. Sorel, "The search for neutrinoless double-beta decay", La Rivista del Nuovo Cimento 46, 619–692 (2023).
- ¹³M. Gavela, T. Hambye, D. Hernández, and P. Hernández, "Minimal flavour seesaw models", Journal of High Energy Physics **2009**, 038–038 (2009).
- ¹⁴P. Coloma and S. Ipek, "Neutrino masses from a pseudo-dirac bino", Physical Review Letters 117, 10.1103/physrevlett.117.111803 (2016).
- ¹⁵C. M. Ayber and S. Ipek, "A hybrid type i + iii inverse seesaw mechanism in u(1)r-l-symmetric mssm", Journal of High Energy Physics **2023**, 10.1007/jhep11(2023)085 (2023).
- ¹⁶Á. González, "Measurement of areas on a sphere using fibonacci and latitude–longitude lattices", Mathematical Geosciences 42, 49–64 (2009).